Numerical Solution of Fields in Lossy Structures Using MAGY

Alexander N. Vlasov, *Member, IEEE,* and Thomas M. Antonsen, Jr., *Member, IEEE*

***Abstract*—Lossy structures are used in vacuum electronic devices to control and suppress modes. Numerical simulation of the effect of these lossy structures is critical to the design and optimization of devices. The gyrotron simulation code MAGY makes use of the generalized telegraphist's equations in which the transverse structure of fields is represented as a sum of local modes of a metallic waveguide. If the wall is not a perfect conductor then sum over modes is not uniformly convergent. We have developed an algorithm to deal with this problem and allow for the simulation of structure with highly lossy walls. The theory and implementation of this algorithm will be presented.**

***Index Terms*—Hybrid codes, lossy structures, microwave tubes.**

I. Introduction

DESIGNING new sources of electromagnetic millimeter wavelength radiation requires extensive computer simulation to reduce design cycles and optimize performance. It is an important requirement for computer codes to be able to describe real processes in vacuum electronic devices [1]. The gyrotron simulation code MAGY [2] developed at the University of Maryland and Naval Research Laboratory is able to describe the self-consistent nonlinear interaction between electromagnetic fields of axisymmetric structures and electron beams. It is particularly useful for millimeter wave device modeling because it can simulate highly overmoded structures. There are many gyrodevices operating in the millimeter and submillimeter wavelengths which contain a variety of loss mechanisms: losses in beam tunnels to suppress electron beam instabilities [3]–[6], lossy ceramic in drift sections to prevent excitation of parasitic modes [4], [6], [7], losses in cavities to control quality factors, and losses due to the presence of slots and holes. Thus, it is imperative to develop a method to treat these effects is MAGY. The presence of partially conducting materials can drastically change the electromagnetic field properties. To predict microwave device operation in the presence of lossy elements we should be able to calculate accurately the electromagnetic fields including the effects of both the losses and the electron beam.

The generalized telegraphist's equations approach [8], [17], [9] and related methods of transverse cross sections [10] are widely used in the theory of waveguides with axially varying boundaries and for electronic device simulations [2], [11]. The effect of wall losses can be treated in a general way, perturbatively, if the value of the surface impedance of the wall is small [12], [18], [13], [14], [19]. This approach is successful for waveguides with highly conducting metal walls. Problems arise when the surface impedance becomes large, which is often the case of interest. To treat this case a computer code should be able to solve the electromagnetic field problem in the case of a partially absorbing wall. The goal of this work is to extend the generalized telegraphist's equations approach for the case of structures with finite wall surface impedance.

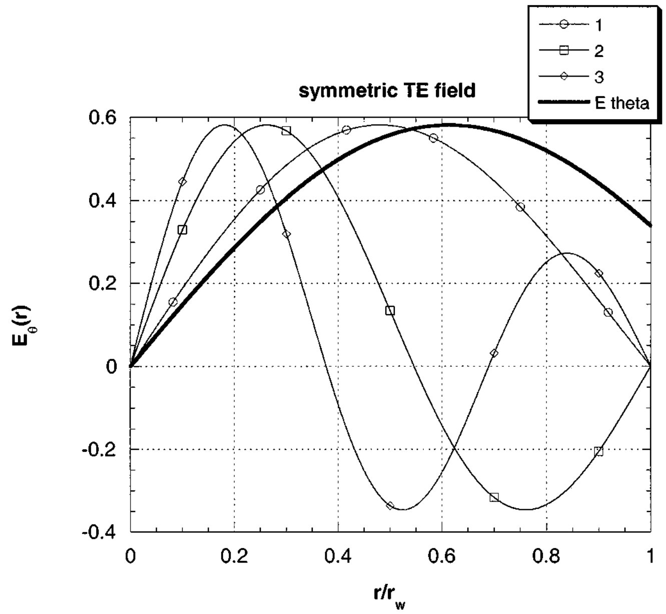

Fig. 1. Radial distribution of electric field E_θ for the three first basis functions and for an actual field in the case of finite wall conductivity.

The nature of the difficulty associated with the generalized telegraphist's equations approach is that the fields are represented as a superposition of waveguide modes appropriate to a structure with perfectly conducting boundaries. For each mode in the superposition the tangential electric field vanishes at the boundary of the simulation region. However, if the boundary, in fact, has nonzero surface impedance, then the actual tangential field will be nonzero at the surface, see Fig. 1 as an illustration. Here we have plotted the theta component of the electric field for the first three symmetric modes of cylindrical waveguide of radius r_w along with a hypothetical field that could be present if the metallic wall where replaced by a surface with large impedance. This field can still be represented as a superposition of perfectly conducting boundary waveguide modes.

Manuscript received June 30, 2000; revised September 12, 2000. This work was supported by the Office of Naval Research and the U.S. Department of Energy. The review of this paper was arranged by Editior D. Goebel.

A. N. Vlasov is with Science Applications International Corporation, 1710 SAIC Dr., McLean, VA 22102 USA, on leave from Moscow State University, Moscow, Russia (e-mail: vlasov@glue.umd.edu).

T. M. Antonsen, Jr. is with the Institute for Plasma Research, University of Maryland, College Park, MD 20742 USA.

Publisher Item Identifier S 0018-9383(01)00301-X.

However, the series will not be uniformly convergent. As a result one can expect Gibbs' phenomenon to appear in any truncation of the series (see as an example [15]), and one can expect that extreme care needs to be taken when taking spatial derivatives of the field. A possible alternative to representing the fields as a superposition of waveguide modes appropriate to a structure with perfectly conducting walls is to consider modes that individually satisfy the boundary conditions at the wall. There are several drawback associated with this idea. First, these modes are more difficult to find than the perfect conducting boundary modes. For example, a nonzero surface impedance couples TE and TM modes. Thus, the basis functions in the nonzero surface impedance case would have mixed polarization. Second, the structure of the modes would be different for and require calculation at each axial location. Using modes appropriate to a perfectly conducting cylinder (Bessel functions) allows us to evaluate the modes by scaling the radial coordinate to the wall radius. Third, if one introduces a real surface impedance, then the self adjoint property of the Maxwell equations is lost, and it is no longer clear that the nonzero surface impedance modes form a complete basis.

Our approach to the problem of nonuniform convergence will be presented in Section II of this paper. Section III contains examples of numerical simulations of different electrodynamic structures with lossy materials on the walls. The summary and discussions about the advantages and limitations of the proposed modifications are presented in Section IV.

II. Basic Formulation for Lossy Structures

One of the most successful approaches to describe electromagnetic fields in complex waveguides and cavities and their interaction with electron beams is based on the representation of the electromagnetic field as a sum of local eigenfunctions of the structure. The MAGY code developed at the University of Maryland is an example of such an approach for the case in which the radiation has a narrow spectral width. A complete derivation of the generalized telegraphist's equations used in MAGY code is presented in ref. [2]. Here, we reproduce some steps, which are necessary in order to formulate a description of the field when the wall has a nonzero surface impedance.

A. Generalized Telegraphist's Equations

The electromagnetic field is split into transverse and longitudinal parts:

$$\mathbf{E}(\mathbf{r}, t) = \mathrm{Re}\{(\mathbf{E_T}(\mathbf{r}, t) + E_z(\mathbf{r}, t)\mathbf{e_z}) \exp(-i\omega t)\} \tag{1a}$$

$$\mathbf{B}(\mathbf{r}, t) = \mathrm{Re}\{(\mathbf{B_T}(\mathbf{r}, t) + B_z(\mathbf{r}, t)\mathbf{e_z}) \exp(-i\omega t)\} \tag{1b}$$

where

$\mathbf{E_T}, \mathbf{B_T}$	complex amplitudes of the transverse electric and magnetic fields;
E_z, B_z	complex amplitudes of the longitudinal field components;
ω	carrier frequency, $k_0 = \omega/c$;
$\mathbf{e}_z$	unit vector directed along the z axis.

The complex field vectors $\mathbf{E_T}$ and $\mathbf{B_T}$ as well as E_z and B_z are assumed to be slowly varying functions of time. The transverse fields are represented at each axial location as a sum of TM, TE and TEM modes (For the current case we limit our analysis to noncoaxial waveguides with TM and TE modes only.) of a waveguide with a transverse cross-section equal to the local transverse cross section of the structure.

$$\mathbf{E_T} = \sum_k \left(V'_k(z, t)\mathbf{e}'_\mathbf{k}(\mathbf{r_T}, z) + V''_k(z, t)\mathbf{e}''_k(\mathbf{r_T}, z)\right) \tag{2a}$$

$$\mathbf{B_T} = \sum_k \left(I'_k(z, t)\mathbf{b}'_\mathbf{k}(\mathbf{r_T}, z) + I''_k(z, t)\mathbf{b}''_k(\mathbf{r_T}, z)\right). \tag{2b}$$

Here, the primed variables refer to TM modes and the double primed variables refer to TE modes. The amplitudes V'_k, V''_k, I'_k and I''_k depend slowly on time and arbitrarily on the axial coordinate z. The two sets of eigenfunctions of the local transverse cross section are introduced as follows:

$$\mathbf{e}'_k = \nabla_\perp \Psi_k \tag{3a}$$

$$\mathbf{b}'_k = \mathbf{e_z} \times \mathbf{e}'_k \tag{3b}$$

where

$$\Delta\Psi_k + k'^2_{C,k}\Psi_k = 0 \tag{3c}$$

$$\Psi_k|_C = 0 \tag{3d}$$

describing TM modes, and

$$\mathbf{b}''_k = \nabla_\perp \Phi_k, \tag{4a}$$

$$\mathbf{e}''_k = \mathbf{b}''_k \times \mathbf{e}_z \tag{4b}$$

where

$$\Delta\Phi_k + k''^2_{C,k}\Phi_k = 0, \tag{4c}$$

$$\mathbf{n} \cdot \nabla\Phi_k|_C = 0 \tag{4d}$$

describing TE modes. The eigenfunctions are orthogonal with normalization

$$\int_{S_\perp} da\mathbf{e}'^*_k \cdot \mathbf{e}'_n = \int_{S_\perp} da\mathbf{e}''^*_k \cdot \mathbf{e}''_n = \delta_{k,n}$$

$$\int_{S_\perp} da\mathbf{e}'^*_k \cdot \mathbf{e}''_n = 0$$

$$\delta_{k,n} = \begin{cases} 1, & \text{if } k = n, \\ 0, & \text{if } k \neq n. \end{cases}$$

Here, C represents the curve defining the boundary of the local cross section in which the fields are represented and $\mathbf{n}$ is an outward normal from this curve. We will characterize the axially varying boundary by the two dimensional vector $\mathbf{r_w}(\theta, z)$. Where the polar angle θ varies from 0 to 2π. We assume that $\mathbf{r_w}(\theta, z)$ is single valued, however this restriction can be dropped later. A unit vector tangent to this curve is $\mathbf{t}_\perp$ where

$$\mathbf{t}_\perp = \frac{\partial \mathbf{r_w}}{\partial \theta} \bigg/ \left|\frac{\partial \mathbf{r_w}}{\partial \theta}\right|$$

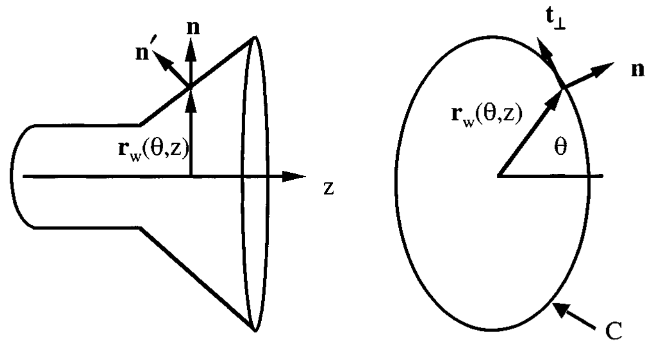

Fig. 2. Coordinates and unit vectors for an axially varying waveguide with an elliptical cross section.

and the outward normal $\mathbf{n}$ is given by $\mathbf{n} = \mathbf{t}_\perp \times \mathbf{e_z}$. Note that the vector $\mathbf{n}$ lies in the transverse plane and is not, in general, normal to the surface defined by the family of axially dependent curves. The situation is illustrated in Fig. 2. On the left we see an axially varying waveguide and on the right we see the cross section of the waveguide at a particular axial point. The cross section pictured is elliptical. The unit vectors $\mathbf{n}$ and $\mathbf{t}_\perp$ lie in the plane of the cross section. The shape of the cross section is defined by the two-dimensional (2-D) vector function $\mathbf{r_w}(\theta, z)$. The normal to the waveguide surface is $\mathbf{n}'$, which, in general, will have a component in the z direction. Finally, we introduce $r'_w(\theta, z) = \mathbf{n} \cdot \partial \mathbf{r_w}/\partial z$ which defines the local rate of change of the radius of a point on the curve C.

The longitudinal components of electromagnetic field are related by Maxwell's equations to the transverse components:

$$ik_0 B_z = \nabla_\perp \cdot (\mathbf{E_T} \times \mathbf{e_z}) \tag{5}$$

and

$$ik_0 E_z = \frac{4\pi}{c} j_z - \nabla_\perp \cdot (\mathbf{B_T} \times \mathbf{e_z}) \tag{6}$$

where j_z is the complex amplitude of the beam current. Thus, if the transverse components are known at each axial position the longitudinal components can be determined from them.

The transverse components of the fields are governed by the transverse components of Maxwell's equations

$$\frac{\partial}{\partial z}\mathbf{E_T} - \nabla_T E_z = ik_0 \mathbf{B_T} \times \mathbf{e_z} \tag{7}$$

and

$$\frac{\partial}{\partial z}\mathbf{B_T} - \nabla_T B_z = \frac{4\pi}{c}\mathbf{j} \times \mathbf{e_z} - ik_0 \mathbf{E_T} \times \mathbf{e_z}. \tag{8}$$

The Maxwell equations written above are appropriate for the case in which the fields are monochromatic. That is the spectrum consists of a single frequency ω, and the complex amplitudes are time independent. We will continue the derivation under this assumption. We can recover at subsequent times the results for slow time variation of the amplitudes by replacing the frequency ω by the operator $(\omega + i\partial/\partial t)$.

To obtain telegraphist's equations one dots (7) with either $\mathbf{e}'_\mathbf{k}$ or $\mathbf{e}''_\mathbf{k}$ and (8) with either $\mathbf{b}'_\mathbf{k}$ or $\mathbf{b}''_\mathbf{k}$ and integrates over the transverse cross section of the waveguide. One then inserts when appropriate the expression [(2a) or (2b)] for the transverse fields, and uses (5) and (6) to eliminate the longitudinal fields. Because of the anticipated nonuniform convergence in the sums in (2a)–(2b) it is critical that transverse derivatives of the fields are not carried out term by term. For example, one can not insert (2a) into (5) and arrive at a series expression for $\mathbf{B}_z$. Rather, in the integrals over transverse cross section, terms involving transverse derivatives must be done by parts so that the transverse derivative falls on the single basis functions $\mathbf{e}^*_\mathbf{k}$ and $\mathbf{b}^*_\mathbf{k}$ and not on the fields themselves. This procedure results in the following pair of equations:

$$\frac{\partial V_k}{\partial z} = \sum_l K_{l,k} V_l + \Delta_k I_k - S_{z,k} + \int_C dl \mathbf{n} \cdot \mathbf{e}^*_\mathbf{k} \left(E_z + r'_w \mathbf{n} \cdot \mathbf{E}_\perp\right) \tag{9}$$

and

$$\frac{\partial I_k}{\partial z} = \sum_l K_{k,l} I_l + \Gamma_k V_k - S_{T,k} - \frac{1}{ik_0}\int_C dl \nabla_\perp \cdot \mathbf{b}^*_\mathbf{k} \mathbf{n} \cdot (\mathbf{E}_\perp \cdot \mathbf{e_z}). \tag{10}$$

The preceding equations apply to either TE or TM amplitudes depending on whether the transverse components of Maxwell's equations were dotted with a primed or double primed basis function. Implicit in the sum over all modes, l, is a sum over mode type, TE and TM. In some instances terms simplify or disappear for one or the other mode types. For example, it follows from (2a)–(2b) that $\nabla_\perp \cdot \mathbf{b}'_k = \nabla_\perp \cdot \mathbf{e}''_k = 0$.

Coefficients appearing in (9) and (10) are defined as follows. The coupling matrix $K_{l,k}$ describes the effect of axial variations of the transverse crosssection of the waveguide, as follows:

$$K_{k,i} = \int_{S_\perp} \mathbf{b}^*_k \cdot \frac{\partial \mathbf{b}_i}{\partial z}\, da = \int_{S_\perp} \mathbf{e}^*_k \cdot \frac{\partial \mathbf{e}_i}{\partial z}\, da.$$

Again we note that the basis functions may be either of the primed (TM) or double primed (TE) type depending on the circumstances. The coefficients Δ_k and Γ_k determine the axial propagation constants for the waveguide modes

$$\Delta_k = \begin{cases} ik_0\left(1 - \dfrac{k'^2_{C,k}}{k_0^2}\right), & \text{for TM modes} \\ ik_0, & \text{for TE modes} \end{cases}$$

$$\Gamma_k = \begin{cases} ik_o, & \text{for TM modes} \\ ik_0\left(1 - \dfrac{k''^2_{C,k}}{k_0^2}\right), & \text{for TE modes} \end{cases}$$

where $k'_{C,k}(z)$ and $k''_{C,k}(z)$ are the axial dependent cut off wave numbers which are the eigenvalues of (3c) and (4c). The quantities $S_{z,k}$ and $S_{T,k}$ are sources in the wave equation describing the excitation of fields by the electron beam

$$S'_{z,k} = \frac{4\pi}{i\omega}\int_{S_\perp} da j_{z,\omega} \nabla_\perp \cdot \mathbf{e}'^*_\mathbf{k}$$

and

$$S'_{T,k} = \frac{4\pi}{c}\int_{S_\perp} da \mathbf{j}_{\mathbf{T},\boldsymbol{\omega}} \cdot \mathbf{e}'^*_\mathbf{k}, \quad S''_{T,k} = \frac{4\pi}{c}\int_{S_\perp} da \mathbf{j}_{\mathbf{T},\boldsymbol{\omega}} \cdot \mathbf{e}''^*_\mathbf{k}.$$

Finally, there are boundary terms involving integrals over the perimeter of the transverse cross section of the waveguide. Both boundary terms involve integrals of the tangential electric field at the perimeter. These terms vanish if the wall is perfectly conducting but are nonzero if the surface of the wall has a nonzero impedance.

B. Evaluation of the Surface Terms

In order to evaluate these terms one must have a method for evaluating fields outside the simulation boundary, $\mathbf{r_w}(\theta, z)$. We will adopt the approximation that each point on the surface is characterized by an impedance such that the tangential electric field is given by

$$\mathbf{E}_s = Z_s \mathbf{B} \times \mathbf{n}' \tag{11}$$

where $\mathbf{n}'$ is the outward normal to the surface

$$\mathbf{n}' = \frac{\mathbf{n} - r'_w \mathbf{e_z}}{(1 + r'^2_w)^{1/2}}. \tag{12}$$

Here, we note the distinction between the normal to the surface defining the simulation, $\mathbf{n}'$, and the normal to the curve defining the local transverse cross section, $\mathbf{n}$. These normals are illustrated in Fig. 2. For the moment we consider the impedance to be isotropic, but later we will allow for it to depend on the direction of flow of the surface current, $\mathbf{B} \times \mathbf{n}'$.

Characterization of fields outside the simulation region by a local impedance is an approximation. In fact, the relationship between magnetic and electric field is nonlocal. A local approximation can be expected to be valid if the thickness of the region being modeled is less than the scale length for axial or lateral variations of the field. This will be discussed in more detail when we consider the particular example of annular dielectric rings in cylindrical cavities.

We now focus on evaluation of the boundary terms in (9) and (10). Using formula (11) for the surface electric field and expression (12) for the normal vector $\mathbf{n}'$ we find,

$$\mathbf{e_z} \cdot \mathbf{E_s} + r'_w \mathbf{n} \cdot \mathbf{E_s} = Z_s \sqrt{1 + r'^2_w}\, (\mathbf{e_z} \times \mathbf{B_T} \cdot \mathbf{n}).$$

What is required for this expression is the tangential component on the boundary of the transverse magnetic field. The series expression (2b) for this component is well behaved. We then substitute the series expression for the transverse magnetic field and arrive at

$$\begin{aligned} &\int dl \mathbf{n} \cdot \mathbf{e}^*_\mathbf{k} \left(E_z + r'_w \mathbf{n} \cdot \mathbf{E_T}\right) \\ &\quad = -\int dl Z_s \sqrt{1 + r'^2_w}\, \mathbf{n} \cdot \mathbf{e}^*_\mathbf{k} \sum_l I_l \mathbf{n} \cdot \mathbf{e_k}. \end{aligned} \tag{13}$$

This expression is easy to implement and does not lead to nonuniform convergence when truncated at a finite number of modes.

The boundary term appearing in (10) is more difficult to implement. We note that due to the factor $\nabla_T \cdot \mathbf{b}^*_k$ this term is nonzero only for TE modes. The boundary term requires evaluation of the component of the electric field in the $\mathbf{t}_\perp = \mathbf{e_z} \times \mathbf{n}$ direction,

$$\mathbf{t}_\perp \cdot \mathbf{E}_\perp = \mathbf{n} \cdot (\mathbf{E}_\perp \times \mathbf{e_z}).$$

For a circular cavity this corresponds to the θ-component of the electric field. Expressing this field in terms of the surface impedance and tangential magnetic field, $\mathbf{E_s} = Z_s \mathbf{B_s} \times \mathbf{n}'$ gives

$$\mathbf{t}_\perp \cdot \mathbf{E}_\perp = \frac{Z_s}{(1 + r'^2_w)^{1/2}} \left(B_z + r'_w \mathbf{n} \cdot \mathbf{B}\right) \tag{14}$$

where we have used expression (12) for the surface normal $\mathbf{n}'$. Equation (14) can not be implemented directly because we do not have a uniformly convergent series for the cross-section normal component of the transverse magnetic field on the boundary, $\mathbf{n} \cdot \mathbf{B}$. In particular, the normal magnetic field vanishes for each term in the sum given by (2b). Instead we express the cross section normal field in terms of the surface normal field

$$\mathbf{n} \cdot \mathbf{B} = \sqrt{1 + r'^2_w}\, (\mathbf{n}' \cdot \mathbf{B}) + r'_w B_z.$$

Thus, we have

$$\mathbf{t}_\perp \cdot \mathbf{E}_\perp = Z_s \lfloor (1 + r'^2_w)^{1/2} B_z + r'_w \mathbf{n}' \cdot \mathbf{B} \rfloor. \tag{15}$$

Evaluation of the surface normal field can be carried out using Faraday's law,

$$\begin{aligned} i\frac{\omega}{c} \mathbf{n}' \cdot \mathbf{B} = &\frac{1}{|\partial \mathbf{r}_w / \partial\theta| \sqrt{1 + r'^2_w}} \\ &\cdot \left[\frac{\partial}{\partial\theta}\left(\mathbf{e}_z + \frac{\partial \mathbf{r}_w}{\partial z}\right) \cdot \mathbf{E} - \frac{\partial}{\partial z}\left(\frac{\partial \mathbf{r}_w}{\partial\theta} \cdot \mathbf{E}\right)\right]. \end{aligned} \tag{16}$$

Combining (15) and (16) results in a differential equation for $\mathbf{t}_\perp \cdot \mathbf{E}_\perp$ that can in principle be integrated. We note that this difficulty is avoided if either the surface impedance is small or if the surface impedance is nonzero only on regions where the wall radius is constant. In either case we may drop the second term on the right side of (15). That is the surface normal magnetic field. We assume that this is the case and proceed.

We now must evaluate B_z, and in particular obtain an expression for B_z on the boundary to be inserted in (15). To represent B_z we write it as a superposition of the basis functions Φ_k used to define TE modes in (4a)–(4b) and (4c)–(4d)

$$B_z(\mathbf{x}_\perp, z) = \sum_{k=0}^{\infty} B_k(z) \Phi_k(\mathbf{x}_\perp, z).$$

Here the sum includes all modes appearing in (2a) as well as the $k = 0$ solution for which $k''^2_{c,0} = 0$ and $\Phi_0 = \Phi_0(z)$ independent of $\mathbf{x}_\perp$. This latter solution does not contribute to the representation of $\mathbf{B}_T$ $(\nabla_\perp \Phi_0 = \mathbf{b}_0 = 0)$ but is necessary in the representation of B_z. The normalization for $\Phi_0(z)$ is chosen to be such that

$$\int_{S_\perp} da\, |\Phi_0|^2 = 1.$$

We now multiply (5) by Φ_k^* and integrate over the cross-section to obtain formulas for the amplitudes B_k,

$$B_k \int da\, |\Phi_k|^2 = \frac{1}{ik_0} \left\{ \int dl \Phi_k^* \mathbf{t}_\perp \cdot \mathbf{E}_\perp + V_k'' \right\}.$$

Using the relation (15) between B_z and the tangential component of the electric field on the boundary results in an integral equation for $\mathbf{t}_\perp \cdot \mathbf{E}_\perp = Z_s(1 + r'^2_w)^{1/2} B_z$,

$$\mathbf{t}_\perp \cdot \mathbf{E}_\perp |_C = \frac{Z_s(1 + r'^2_w)^{1/2}}{ik_0} \sum_{k=0}^{\infty} \frac{\Phi_k|_C}{\int da\, |\Phi_k|^2} \cdot \left\{ \int dl \Phi_k^* \mathbf{t}_\perp \cdot \mathbf{E}_\perp + V_k'' \right\}.$$

This equation must be satisfied at each axial point in the simulation region. It has the form of an integral equation in which the function $\mathbf{t}_\perp \cdot \mathbf{E}_\perp$ is determined from the known value of V_k'', the TE mode voltages. This equation has some very peculiar features. First, the usual perturbative technique for calculating wall losses consists of assuming Z_s is small and dropping the integral kernel on the right hand side. One then obtains directly on expression for $\mathbf{t}_\perp \cdot \mathbf{E}_\perp$ which is proportional to the surface impedance and the TE voltages. The peculiar feature is that the integral kernel diverges in the case when the sum over modes is not truncated. (Thus, the perturbative technique requires dropping a term, which is infinite.) The divergence can be seen by realizing that for high order modes the value of Φ_k on the boundary is essentially the same as the value of Φ_k in the interior of the cross section. Thus, each term in the sum scales as the perimeter divided by the cross-sectional area, and the sum does not converge. Implementation of (16) with a truncated set of modes will yield results that depend on the number of modes included, which is clearly unsatisfactory. In spite of this apparent difficulty (16) is still valid. Convergence of the sum occurs because the quantity in the curved brackets tends to zero as $k \to \infty$. This follows from (10), which we rewrite for TE modes

$$V_k'' = \frac{1}{k''^2_{C,k} - k_0^2} \left[-k''^2_{C,k} \oint_C \Phi_k^*(r_w) \mathbf{t}_\perp \cdot \mathbf{E}\, dl + ik_0 L_k \right] \tag{17}$$

where

$$L_k = \frac{\partial I_k''}{\partial z} + \sum_l K_{k,l} I_l + S''_{T,k}$$

and we have used the definition of Γ_k appearing in (10). Thus, as

$$k \to \infty \left(k''^2_{C,k} \gg k_0^2\right) V_k'' \to -\oint_C \Phi_k^*(r_w) \mathbf{t}_\perp \cdot \mathbf{E}\, dl_\perp.$$

Here we have assumed the L_k does not diverge with mode number k.

To realize a convergent solution of (16) and (17) we separate the modes into two classes: active and passive. The active modes are the low order modes ($k \le k_{\max}$) for which we solve the telegraphist's equation (10) numerically. The passive modes are the remaindering modes ($k > k_{\max}$) for which we solve (17) for V_k'' keeping only the terms that are important in the limit $k \to \infty$, that is we neglect L_k. With this separation of modes our boundary integral equation for $\mathbf{t}_\perp \cdot \mathbf{E}_\perp$ can be rewritten

$$\begin{aligned} &\frac{ik_0}{Z_s(1 + r'^2_w)^{1/2}} \mathbf{t}_\perp \cdot \mathbf{E}_\perp - \sum_{k=0}^{k_{\max}} \\ &\cdot \frac{\Phi_k(r_w) \oint dl \Phi_k^*(r_w) \mathbf{t}_\perp \cdot \mathbf{E}_\perp}{\int da\, |\Phi_k|^2} + \sum_{k_{\max}+1}^{\infty} \\ &\cdot \frac{k_0^2 \Phi_k(r_w) \oint dl \Phi_k^*(r_w) \mathbf{t}_\perp \cdot \mathbf{E}_\perp}{(k''^2_{C,k} - k_0^2) \int da\, |\Phi_k|^2} \\ &= \sum_{k=0}^{k_{\max}} \frac{\Phi_k V_k''}{\int da\, |\Phi_k|^2}. \end{aligned} \tag{18}$$

The third term on the left side converges due to the factor $k''^2_{C,k}$ in the denominator. This equation can thus be inverted to find $\mathbf{t}_\perp \cdot \mathbf{E}_\perp$ from a given set of active modes. Convergence with respect to the number of active modes is also assured. Increasing $k_{\max}$ changes both the left and right hand sides of (18). However, if $k_{\max}$ is sufficiently large so as to fall in the asymptotic range of (17), then the resulting value of $\mathbf{t}_\perp \cdot \mathbf{E}_\perp$ is unchanged.

C. Telegraphist's Equations for a Structure with Circular Cross Section

Implementation of (18) for the case of a structure with circular cross-section is straightforward. In this case the basis functions Φ_k are ordinary Bessel functions

$$\Phi_k = C_k J_n(k''_{C,k} r) e^{\mathrm{in}\theta}$$

where $k''_{C,k} = j'_{n,k}/r_{wall}(z)$, and $C_k = 1/(J_n(j'_{n,k}) [\pi(j'^2_{n,k} - n^2)]^{1/2})$. Equation (18) then reduces to an algebraic relation for $\mathbf{t}_\perp \cdot \mathbf{E}_\perp$. The final form of (10) for active TE modes then is given by

$$\begin{aligned} \frac{2}{c} \frac{\partial V_k''}{\partial t} =& \Gamma_k'' V_k'' - \frac{\partial I_k''}{\partial z} - \sum_l K_{k,l} I_l \\ &+ Z_V \alpha_k \sum_l \alpha_l V_l'' - S''_{T,k} \end{aligned} \tag{19}$$

where

$$Z_V = \frac{2}{ik_0 r_w^3 D}, \qquad \alpha_k = \frac{j'^2_{n,k}}{\sqrt{j'^2_{n,k} - n^2}}$$

and the constant D is essentially the operator appearing at the left hand side of (18).

$$\begin{aligned} D =& \frac{ik_0}{Z_s \sqrt{1 + r'^2_w}} - 2\pi r_w \sum_{k=1}^{k_{\max}} k^2_{C,k} |\Phi_k(r_w)|^2 \\ &+ 2\pi r_w \sum_{k_{\max}+1}^{\infty} |\Phi_k(r_w)|^2 \frac{k_0^2 k^2_{C,k}}{k^2_{C,k} - k_0^2} - \frac{2}{r_w} \delta_{0,n} \end{aligned}$$

$$Z_s = E_\theta / B_z = Z_s^{\mathrm{TE}}.$$

Note that, as discussed previously, we have restored the time derivative to the voltage in (19). This comes from the frequency dependence of Γ_k'' via the replacement $\omega \to (\omega + i\partial/\partial t)$ and assuming $|\partial/\partial t| \ll \omega$. The telegraphist's equations after substitution of all lossy terms can be written in the following form:

$$\begin{aligned}\frac{2}{c}\frac{\partial V_k''}{\partial t} =& \Gamma_k'' V_k'' - \frac{\partial I_k''}{\partial z} - \sum_l K_{k,l} I_l \\ &+ Z_V \alpha_k \sum_l \alpha_l V_l'' - S_{T,k}'', \end{aligned} \tag{20a}$$

$$\begin{aligned}ik_0 I_k'' =& \frac{\partial V_k''}{\partial z} - \sum_l K_{lk} V_l + Z_I \beta_k \sum_l \beta_l I_l'' \\ &- i Z_I \beta_k \sum_l I_l', \end{aligned} \tag{20b}$$

$$\begin{aligned}\frac{2}{c}\frac{\partial I_k'}{\partial t} =& \Gamma_k' I_k' - \frac{\partial V_k'}{\partial z} - \sum_l K_{l,k} V_l - Z_I \sum_l I_l'' \\ &- i Z_I \sum_l \beta_l I_l'' - S_{z,k}, \end{aligned} \tag{20c}$$

$$ik_0 V_k' = \frac{\partial I_k'}{\partial z} + \sum_l K_{kl} I_l + S_{T,k}'' \tag{20d}$$

where $\beta_k = n/\sqrt{j'^2_{n,k} - n^2}$, $Z_I = 2Z_s^{\mathrm{TM}}\sqrt{1 + r'^2_w}/r_w$, the Z_s^{TM} impedance is determined by the ratio E_z/B_θ at the surface. The remainder of this paper will be devoted to illustrating solutions of example problems.

III. Numerical Simulations of Electromagnetic Fields in Lossy Structures

To analyze situations with lossy structures the MAGY code was modified as outlined in the previous section. In this section we present some sample solutions.

A. *Cylindrical Cavity with Nonzero Surface Impedance*

The first numerical test was performed for the simplest geometry of a cylindrical cavity lined by a wall with a nonzero surface impedance. The cavity had a length of 2.0 cm, a radius of 0.4115 cm, the two end plates were perfectly conducting. The inner cylindrical surface of the cavity was given an impedance $Z_s = E_\theta/B_z = (1 - i)$ [corresponding to $Z_s = 377(1 - i)\ \Omega$ in MKS units]. Equations (20a)–(20d) are then solved on a grid in z as described in an earlier paper [2]. The amplitudes of the modes are specified to have a Gaussian dependence on z initially and the time evolution of modes is determined by the code. Because of the large value of surface impedance fields decay rapidly in the time. By plotting the amplitude of modes versus time we determine the decay rate of lowest order axial mode. Fig. 3 displays the dependence of the calculated decay rate γ on the time step Δt for the case of 20 "active" modes. With the smallest time step ($\Delta t = 10^{-13}$ sec.) the real and imaginary parts of the frequency were given by $\omega_0 = 2.76\ 10^{11}$ sec^{-1} and $\gamma_0 = 1.865\ 10^{10}$ sec^{-1} (this corresponds to a normalized frequency $\omega_0\,\Delta t = 0.0276$ and $\gamma_0 \Delta t = 0.001\,87$). In Fig. 3 the time step is normalized to the frequency ω_0. It can be seen from the linear dependence of decay rate on time step

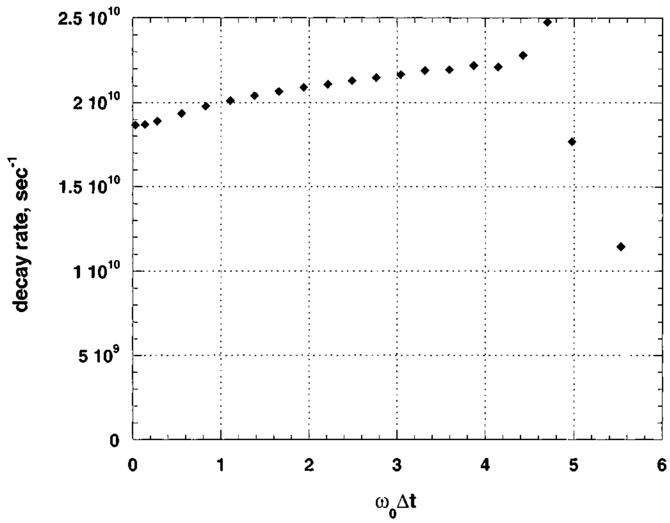

Fig. 3. Decay rate as a function of time step for 20 "active" modes in a closed resonator with a lossy wall ($L = 2$ cm, frequency is 44.0 GHz, $r_w = 0.4115$ cm, $Z_s = 1.0$).

(for small time steps) that the error is first order in the time step. This is due to the fact that the time derivatives in the numerical implementation are slightly forward differenced to achieve stability. We note that reasonably accurate results are obtained even when $\omega_0\Delta t \sim 1$. This shows the computational advantage of the slowly varying envelope approximation. In the present calculation the relative error scales as

$$\frac{(\gamma(\Delta t) - \gamma_0)}{\gamma_0} = 0.034\omega_0\Delta t. \tag{21}$$

Convergence of the decay rate with number of modes simulated is as follows. The simulated decay rates with 1, 5, 10 and 20 modes were 2.787 10^{10}, 1.996 10^{10}, 1.9095 10^{10} and 1.865 10^{10} sec^{-1}. This suggests an error, which scales inversely with the number of active modes. Although the problem of the decay rates for electromagnetic modes of a cylindrical cavity with nonzero surface conductivity can be solved analytically, a comparison with the solution of (20a)–(20d) is not illuminating. This is because (20a)–(20d) are derived under assumption of slow time evolution, whereas the calculated decay rates with $Z_s = (1.0 - i)$ are large and do not satisfy this assumption. The analytic decay rate for this case is $2.4464 \cdot 10^{10}$ sec^{-1}. We have verified that for smaller surface impedance $(Z_s \sim 0.1)$ the computed damping rates agree within 2%

$$\begin{aligned}\big(&\gamma_{\mathrm{MAGY}} = 6.93 \times 10^{10}\ \text{sec}^{-1}, \\ &\gamma_{analytical} = 7.1032 \times 10^{9}\ \text{sec}^{-1}\big)\,.\end{aligned}$$

The important point to consider is that the solutions of interest will be slowly varying in time. For this reason we study driven solutions in the next sections.

B. *Beam Tunnel for Parasitic Mode Suppression*

A more appropriate test of the code is the calculation of field profiles excited by a source with specified frequency. In this regard calculations were performed for beam tunnels designed for parasitic mode suppression. The first beam tunnel considered is one that has been designed at the Naval Research Laboratory [16]. It consists of a periodic array of copper and lossy dielectric rings. The dimensions are as follows: period, $d = 1.15$ cm, length of dielectric rings, $s = 1.0$ cm, depth of dielectric rings, $\Delta r = 0.14$ cm, internal radius, $a = 0.5495$ cm , dielectric constant was $\varepsilon = 11.0 + i2.2$. To calculate the spatial decay rate for waves in a periodic lossy structure we use a long structure with 20 periods and apply outgoing boundary conditions at both ends of the structure. The electromagnetic waves were excited inside the lossy structure by placing a small current source for a selected mode at the center of a periodic structure. The longitudinal size of the current source calculated as the half width of a Gaussian profile, is 0.075 cm.

The presence of the dielectric rings was simulated by placing a finite value of surface impedance at the inner radial position of the dielectric. The values of Z_I and Z_V in Eqs. (20a)–(20d) are determined from the ratios of E_z/B_θ and E_θ/B_z at the inner surface of dielectric rings. For a dielectric ring these values will be unequal. That is, the surface impedance is anisotropic. To determine the appropriate values of the surface impedances we must solve Maxwell's equations in the dielectric rings, subject to the boundary condition that tangential electric field vanishes at the outer radius of the rings where they abut a highly conducting surface. The general form of the solution for the fields involves Bessel functions with arguments $k_\perp r$ where $k_\perp = \sqrt{\varepsilon\omega^2/c^2 - k_z^2}$. In particular we find for the ratio E_z/B_θ

$$Z_s^{\mathrm{TM}} = -\frac{E_z}{B_\theta}\bigg|_{r=r_w} = \frac{1}{\sqrt{\varepsilon}}\left[i\,\frac{H_n^{(1)}(x_d) + \rho_{\mathrm{TM}} H_n^{(2)}(x_d)}{H'^{(1)}_n(x_d) + \rho_{\mathrm{TM}} H'^{(2)}_n(x_d)}\right] \tag{22}$$

where

$$\rho_{\mathrm{TM}} = -\frac{H_n^{(1)}(x_w)}{H_n^{(2)}(x_w)}$$

and we find for the ratio B_z/E_θ

$$Z_s^{\mathrm{TE}} = \frac{E_\theta}{B_z}\bigg|_{r=r_w} = \frac{1}{\sqrt{\varepsilon}}\left[-i\,\frac{H'^{(1)}_n(x_d) + \rho_{\mathrm{TE}} H'^{(2)}_n(x_d)}{H_n^{(1)}(x_d) + \rho_{\mathrm{TE}} H_n^{(2)}(x_d)}\right] \tag{23}$$

where

$$\rho_{\mathrm{TE}} = -\frac{H'^{(1)}_n(x_w)}{H'^{(2)}_n(x_w)}.$$

Here, $x_w = k_\perp(a+\Delta r)$ and $x_d = k_\perp a$, and ε is the complex dielectric permittivity, $H_n^{(1)}(x)$, $H_n^{(2)}(x)$ are Hankel functions of the nth order and first and second kinds, respectively. The notation TM and TE refers to the polarization of the solutions in the dielectric. The fact that (22) and (23) are different implies that the surface impedance of the dielectric is anisotropic. Note that for nonsymmetric solutions of (20a)–(20d) TM and TE modes are coupled together. The transverse wave number $k_\perp$ appearing in the arguments of the Bessel functions depends on k_z which is not defined unambiguously. Presumably it is determined by the longitudinal dependence of the fields in the simulation region, which are not yet known. However, if $\varepsilon\omega^2/c^2 \gg k_z^2$ and the arguments of the Bessel functions are not too large then k_z may be

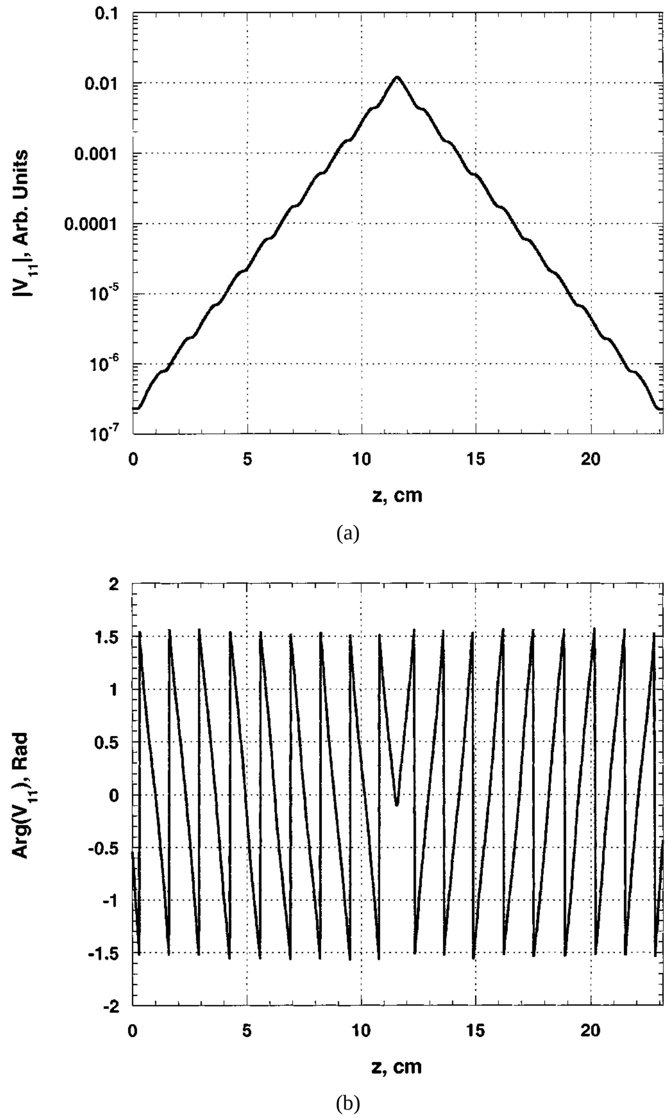

Fig. 4. Dependencies of electromagnetic field amplitude (a) and phase (b) on axial distance for the NRL beam tunnel [16] at a frequency 30 GHz.

neglected. But more specifically, this is the condition for which one can define a local surface impedance. One instance in which the preceding approximation may not hold is if there are resonant solutions with large k_z and fields trapped in the dielectric. For the current case of dielectric rings with high losses these trapped fields should be negligible, but, in general, the problem of trapped fields requires additional analysis.

To excite the desired mode at a prescribed frequency we used a smooth temporal envelop for the source, and run the simulation sufficiently long to verify that we have reached a steady-state solution at the desired frequency. The selected total length of structure (20 periods) was long enough to provide large spatial damping of the electromagnetic field and to minimize the effect of reflection from both ends. The typical dependence of electromagnetic field amplitude and the phase on axial distance is presented in the Fig. 4. It can be seen in the figure that there is region of space where exponential decay of the magnitude accompanied by linear increase in the phase occurs. To find the value of the spatial decay rate we select two points placed at one period separation and form the ratio of

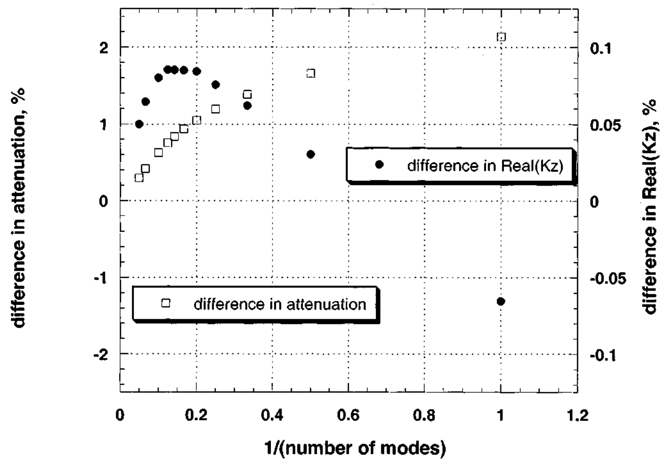

Fig. 5. Relative deviation in attenuation $[\alpha(n) - \alpha(\infty)]/\alpha(\infty)$ and wave number $[k_z(n) - k_z(\infty)]/k_z(\infty)$ as a function of $1/n$, where n is the number of "active" modes for the NRL beam tunnel [16] at frequency 30 GHz.

the field magnitude at these two points. The phase dependence on axial distance is linear (for the most case) inside the region of field damping. Thus we determine the real part of the axial wavenumber, k_z, from the rate of change of phase. So, in this region one can determine the real and imaginary part of the axial wavenumber.

We first investigate the dependence of the calculated wave number on the number of active modes. Fig. 5 displays the dependence of the calculated real and imaginary parts of the wave number as a function of the number of active modes retained in the calculation. The comparison is made for the frequency of 30 GHz. Plotted is the relative deviation in attenuation and wave number from the values, which would be obtained with an infinite number of active modes. These later values are obtained by extrapolating values obtained with large number of modes assuming convergence is realized inversely with the number of modes as suggested in the figure. As can be seen, accuracy of 1% for attenuation and 0.07% for wavenumber is achieved with as few as five modes.

Fig. 6(a) and (b) show the real wave number and attenuation computed over a range of frequencies using five active modes. The solid curves are the values obtained independently via a mode matching technique using the code DRING [16]. The squares are the results of the MAGY calculations. Good agreement is obtained. The major source of error in this process is the determination of the wave number from the MAGY fields.

Nonsymmetric modes in the periodic copper-lossy dielectric tunnel demonstrated similar behavior, as did the symmetric ones. The calculated values of the attenuation and the real part of k_z are plotted in Fig. 7(a), (b) for the least damped, nonsymmetric, hybrid TE_{11}–TM_{11} mode. Both TE and TM "active" modes were used in simulations for this case. The attenuation increases greatly in a narrow frequency band near 20 GHz. In this range of frequencies the transverse mode profile differs qualitatively from that at higher frequencies. Fig. 8 shows the radial dependence of the theta component of the electric field amplitude E_θ where, $\tilde{E}_\theta = \mathrm{Re}\{E_\theta(r, z)e^{i(\theta - \omega t)}\}$ evaluated at the axial location in the middle of a dielectric ring for two

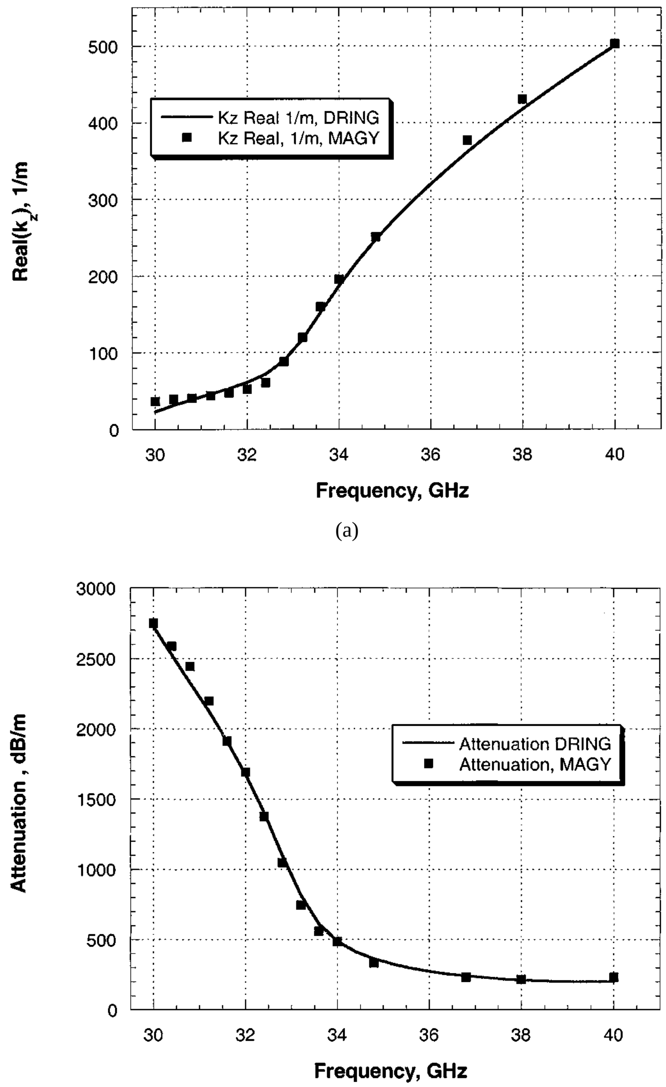

(a)

(b)

Fig. 6. Wavenumber (a) and attenuation (b) as a function of frequency for the TE_{01} mode in the NRL beam tunnel [16] (5 "active" modes).

different frequencies 30.358 GHz, Fig. 8(a), and 19.8 GHz, Fig. 8(b). At the higher frequency [Fig. 8(a)] the radial profile is very similar to that of a mode in a cylindrical, conducting waveguide. At the frequency where attenuation is larger the plot of the field suggests that the field components in the dielectric are relatively large. The calculations employed here used 20 "active" modes of each type. Gibbs' phenomenon associated with the large value of electric field at the surface is evident in the figure. Nevertheless, the calculated decay rate is well converged.

C. Beam Tunnel for Electron Beam Instability Suppression

The second beam tunnel we analyzed has a wall profile chosen to suppress electron beam instabilities, see [3]. The beam tunnel consists of alternating cooper and lossy dielectric rings and is illustrated in Fig. 9. Shown in the figure is the simulation boundary for our calculations. Portions of the boundary alternate between highly conducting metal and lossy

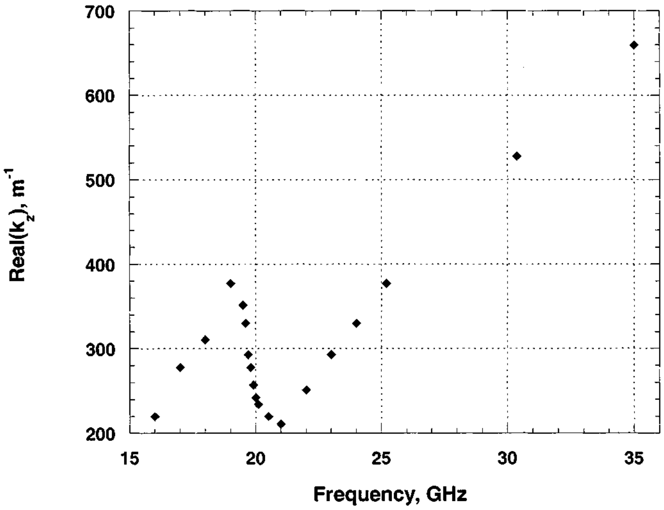

(a)

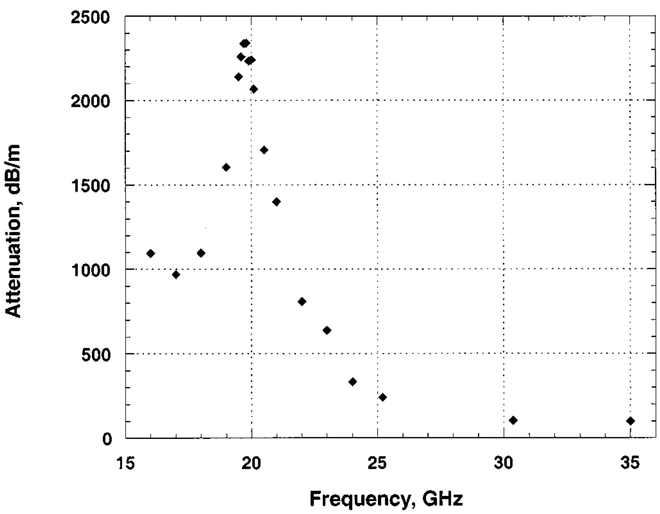

(b)

Fig. 7. Wavenumber (a) and attenuation (b) as a function of frequency for hybrid TM_{11}–TE_{11} mode in NRL beam tunnel [16] (5 “active” modes).

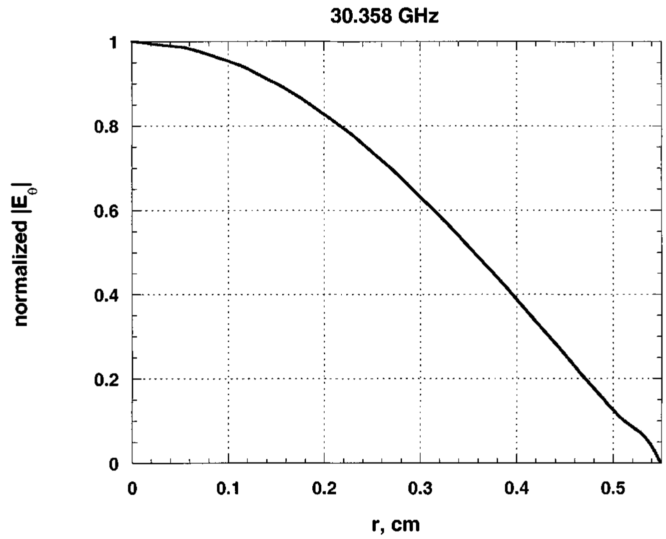

(a)

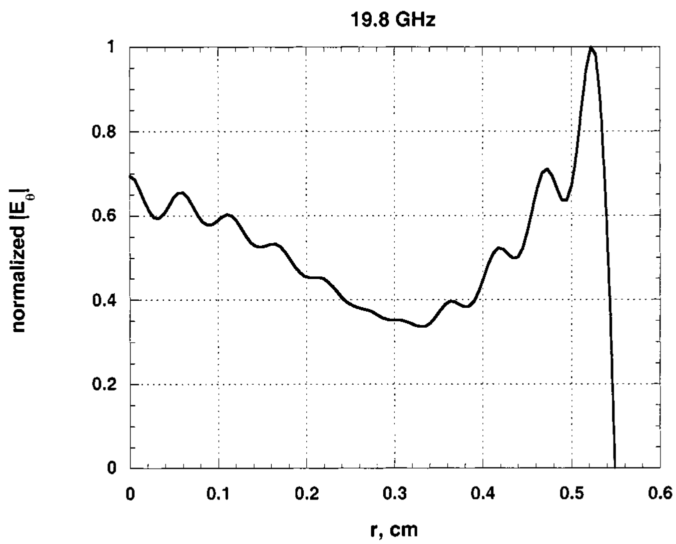

(b)

Fig. 8. The radial dependence of the amplitude of the E_θ field in the middle of a dielectric ring at frequency 30.358 GHz (a) and 19.8 GHz (b) (20 “active” TE and 20 “active” TM modes).

dielectric. In all these are 43 metal rings and 44 dielectric rings. At each end of the structure is a smooth conducting waveguide and outgoing wave boundary conditions are applied at each end. In general the lossy dielectric corresponds to the recessed portions of the boundary where the radius of the boundary is locally maximum. The surface impedance for the dielectric is calculated according to (22) and (23). The minimum and maximum radii of the dielectric rings are 6 mm and 10 mm respectively, the thickness is 3 mm and the dielectric constant $\varepsilon = 5.72 + i0.332$. The boundary at the outer radius of the dielectric is assumed to be perfectly conducting. The minimum radius of cooper rings is 5 mm, and their thickness is 2 mm.

To excite an electromagnetic field in the structure a small field source was placed in the middle of structure. The calculated distribution of field magnitude is presented in Fig. 10 for frequency 86 GHz. It is clear from the figure that the field is localized near the source and almost all power is absorbed by the dielectric rings. More detailed studies of these structures including their excitation by electron beams will be subject of future study.

IV. Conclusions and Discussions

The formulation of the electromagnetic field problem based on the generalized telegraphist’s equations has been improved to allow for simulations of the electromagnetic fields in structures with large surface impedance on the walls. The key steps in the formulation are the recognition that the series representation of the fields is not uniformly convergent and the separation of modes into active and passive groups. The improved formulation has been implemented in the simulation code MAGY. We find that reasonably accurate solution can be obtained even for complex structures with from five to 20 active modes. The numerical stability, convergence and accuracy of developed approach have been analyzed. It is necessary to note that the developed model assumes that the lossy materials can be characterized by a local surface impedance. This is a reasonable approximation in many instances. However, the validity of this approx-

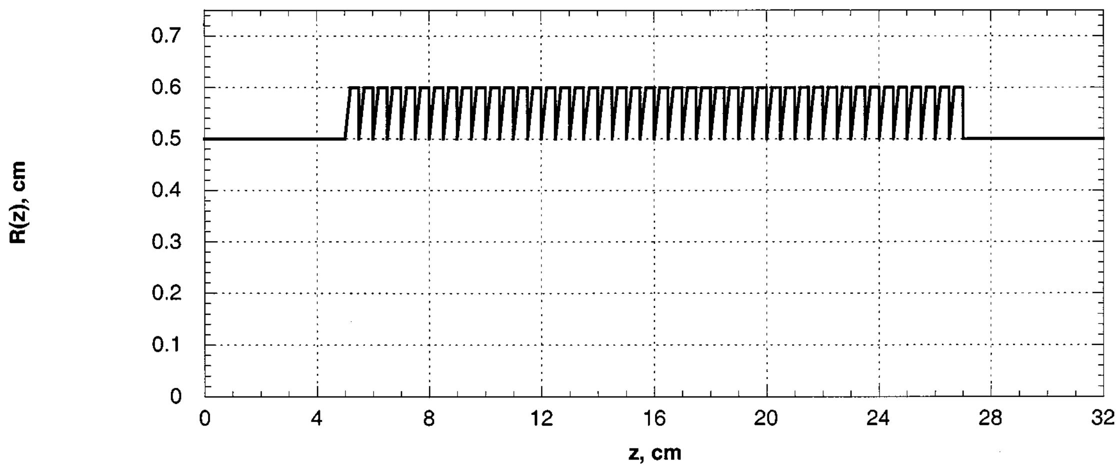

Fig. 9. Profile of beam tunnel radius [3] used in numerical simulations.

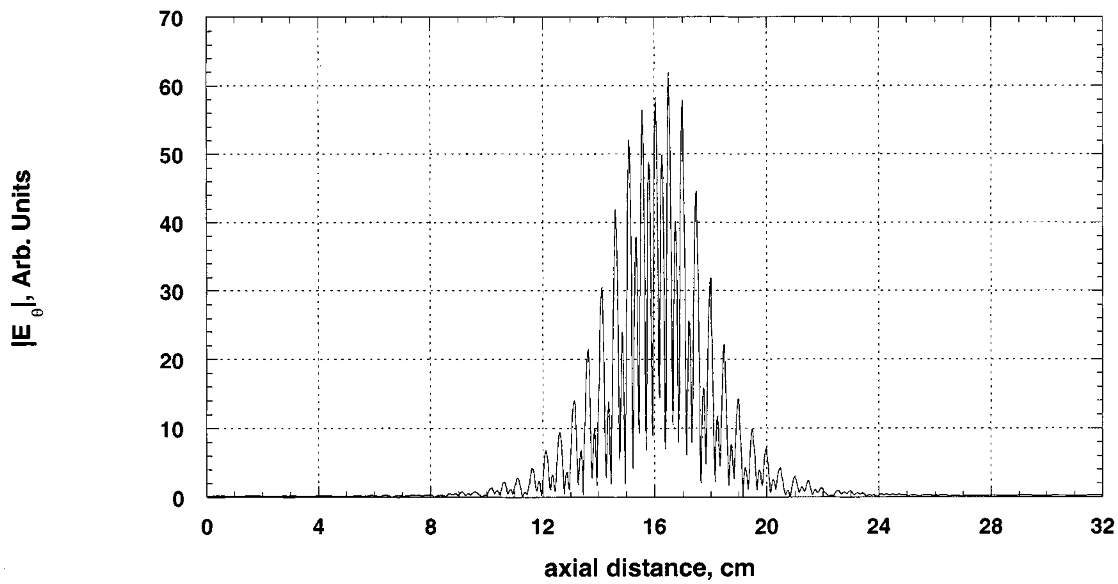

Fig. 10. Dependencies of the E_θ component on axial coordinate for the structure described in Fig. 9 at frequency 86 GHz.

imation must be evaluated on case by case basis. The new capability offered by the code will allow for the design and study of the stability of beam tunnels as well as the suppression of modes in cavities and interaction circuits.

ACKNOWLEDGMENT

The authors are deeply grateful to Dr. J. Calame of the Naval Research Laboratory for his valuable suggestions and his stimulating discussions.

REFERENCES

[1] T. M. Antonsen Jr., A. A. Mondelli, B. Levush, J. P. Verboncoeur, and C. K. Birdsall, "Advances in modeling and simulation of vacuum electronic devices," *Proc. IEEE*, vol. 87, no. 5, pp. 804–839, 1999.

[2] M. Botton *et al.*, "MAGY: A time-dependent code for simulations of slow and fast microwave sources," *IEEE Trans. Plasma Sci.*, vol. 26, pp. 882–892, 1998.

[3] M. Pedrozzi *et al.*, "Electron beam instabilities in gyrotron beam tunnels," *Phys. Plasmas*, vol. 5, pp. 2421–2430, 1998.

[4] J. P. Calame and D. K. Abe, "Applications of advanced materials technologies to vacuum electronics devices," *Proc. IEEE*, vol. 87, pp. 840–864, May 1999.

[5] S. G. Tantawi *et al.*, "High-power X-band amplification from an overmoded three-cavity gyroklystron with a tunable penultimate cavity," *IEEE Trans. Plasma Sci.*, vol. 20, pp. 205–215, June 1992.

[6] J. P. Calame and W. G. Lawson, "A modified method for producing carbon-loaded vacuum compatible microwave absorbers from a porous ceramic," *IEEE Trans. Electron Devices*, vol. 38, pp. 1538–1543, June 1991.

[7] J. P. Calame *et al.*, "Experimental studies of bandwidth and power production in a three cavity, 35 GHz gyroklystron amplifier," *Phys. Plasmas*, vol. 6, no. 1, pp. 285–297, 1999.

[8] G. Reiter, "Generalized telegraphist's equation for waveguides of varying cross-section," in *Proc. Conv. Long Distance Transmission by WaveGuide*, 1959, pp. 54–57.

[9] S. A. Schelkunoff, "Conversion of Maxwell's equations into generalized telegraphist's equations," *Bell Syst. Tech. J.*, vol. 34, pp. 995–1043, 1955.

[10] A. S. Il'insky and A. G. Sveshnikov, "Methods of studying irregular waveguides," *USSR Comput. Maths., Math. Phys.*, vol. 8, pp. 363–373, 1968.

[11] V. M. Pikunov and I. A. Chernyavsky, "Amplification and generation of microwave in relativistic Cherenkov device," *J. Commun. Technol. Electron.*, vol. 38, p. 1, 1993.

[12] A. S. Il'inskiy and G. Ya. Slepyan, "Impedance boundary conditions and their application for calculating the absorption of electromagnetic waves in conducting media," *Sov. J. Commun. Tech. Electron.*, vol. 35, pp. 1–18, 1990.

[13] ——, *Oscillations and Waves in Electrodynamic Structures with Losses* (in Russian). Moscow, Russia: Publish. House Moscow State Univ., 1983.

[14] E. A. Al'khovsky, A. S. Il'insky, and G. I. Troshin, "Computation of phase and attenuation coefficients of electromagnetic waves in a circular, corrugated waveguide," *Sov. J. Commun. Tech. Electron.*, vol. 20, pp. 14–18, 1975.
[15] E. T. Whittaker and G. N. Watson, *A Course of Modern Analysis*, 4th ed. Cambridge, U.K.: Cambridge Univ. Press, 1965, p. 193.
[16] J. Calame, private communication.
[17] G. Reiter, "Generalized telegraphist's equation for waveguides of varying cross-section," *Proc. Inst. Elect. Eng.*, Sept. 1959.
[18] A. S. Il'inskiy and G. Ya. Slepyan, "Impedance boundary conditions and their application for calculating the absorption of electromagnetic waves in conducting media," *Radiotek Eelectron.*, vol. 35, pp. 1121–1139, 1990.
[19] E. A. Al'khovsky, A. S. Il'insky, and G. I. Troshin, "Computation of phase and attenuation coefficients of electromagnetic waves in a circular, corrugated waveguide," *Radiotek. Eelectron.*, vol. 30, pp. 2250–2255, 1975.

Alexander N. Vlasov (M'95) was born in Lipetskaya Oblast, Russia, in 1958. He received the B.Sc. (with honors), M.S., and Ph.D. degrees in physics from Moscow State University, Moscow, Russia, in 1981, 1986 and 1987, respectively.

After graduation, he was Research Scientist from 1986 to 1991, an Assistant Professor from 1991 to 1995, and Associate Professor since 1995 at Department of Physics of Moscow State University. From 1991 to 1998, he was Visiting Scientist at Institute for Plasma Research, University of Maryland, College Park. In 1999, he joined Science Applications International Corporation, McLean, VA. His current research interests include the theory, computer simulations, and design of high-power sources of coherent microwave and millimeter wave radiation, computational methods in diffraction theory, and the theory of electromagnetic fields in complex media.

Thomas M. Antonsen, Jr. (M'87) was born in Hackensack, NJ, in 1950. He received the B.S. degree in electrical engineering in 1973, and the M.S. and Ph.D. degrees in 1976 and 1977, all from Cornell University, Ithaca, NY.

He was a National Research Council Post-Doctoral Fellow at the Naval Research Laboratory, Washington, DC, in 1976 and 1977, and a Research Scientist in the Research Laboratory of Electronics, Massachusetts Institute of Technology, Cambridge, from 1977 to 1980. In 1980, he joined the University of Maryland, College Park, where he joined the faculty of the departments of Electrical Engineering and Physics in 1984. He is currently Professor of Physics and Electrical Engineering. He has held visiting appointments at the Institute for Theoretical Physics, UCSB, the Ecole Polytechnique Federale de Lausanne, Switzerland, and the Institute de Physique Theorique, Ecole Polytechnique, Palaiseau, France. His research interests include the theory of magnetically confined plasmas, the theory and design of high power sources of coherent radiation, nonlinear dynamics in fluids, and the theory of the interaction of intense laser pulses and plasmas. He is the author and co-author of over 180 journal articles and co-author of the book *Principles of Free-Electron Lasers.*

Prof. Antonsen has served on the editorial board of *Physical Review Letters*, *The Physics of Fluids*, and *Comments on Plasma Physics*. He was elected Fellow of the Division of Plasma Physics of the American Physical Society in 1986.